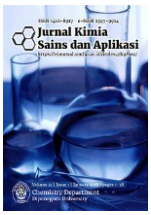
ISSN: 1410-8917
Jurnal Kimia Sains & Aplikasi
e-ISSN: 2597-9914

Jurnal Kimia Sains dan Aplikasi 29 (9) (2026): 648-664

Jurnal Kimia Sains dan Aplikasi
Journal of Scientific and Applied Chemistry

Journal homepage: http://ejournal.undip.ac.id/index.php/ksa



Enhancement of Chitosan Hemodialysis Membranes: Structural Modification with Dicarboxylic Acids and Thickness Control to Improve Performance and Hemocompatibility

Nisrina Salsabila [1], Retno Ariadi Lusiana [1,*], Rahmad Nuryanto [1], Khabibi [1]

[1] Chemistry Department, Faculty of Science and Mathematics, Universitas Diponegoro, Semarang, Indonesia

* Corresponding author: retno.lusiana@live.undip.ac.id

https://doi.org/10.14710/jksa.29.9.648-664

Article Info

Article history:

Received: 31st July 2026
Revised: 13th October 2026
Accepted: 22nd October 2026
Online: 30th October 2026

Keywords:
chitosan membrane; dicarboxylic acid; PEG; dialysis; hemocompatibility

Abstract

Chitosan-based membranes comprising pristine chitosan (CS), PEG 4000-blended chitosan (CP), and PEG 4000-blended chitosan crosslinked with malonic acid (COP), malic acid (CAP), and adipic acid (CDP) were prepared at casting volumes of 5, 7.5, and 10 mL for potential hemodialysis applications. This study evaluated the effects of PEG blending, crosslinker type, and membrane thickness on physicochemical properties, solute transport, and hemocompatibility. FTIR analysis revealed changes in O–H, N–H, C=O, and C–N bands, suggesting hydrogen bonding between chitosan and PEG and ionic interactions between protonated amino and carboxylate groups. Zeta potential values ranged from +55.8 to +74.58 mV. AFM analysis showed that CAP had the highest average roughness (Ra) and root-mean-square roughness (Rq), whereas CDP exhibited the highest maximum height (Rz). PEG blending and dicarboxylic acid crosslinking improved porosity, swelling, water uptake, pH stability, and biodegradability. Increasing casting volume increased membrane thickness, mechanical properties, porosity, and swelling but decreased 6-hour water uptake and solute transport, potentially due to longer diffusion pathways. The 5 mL CAP membrane achieved the highest solute transport, with urea transport increasing from 28.06% for CS to 61.16% and creatinine transport from 14.34% for CS to 49.68%. The modified membranes also retained larger molecules, including vitamin B12 and bovine serum albumin (BSA). The CAP membrane exhibited the lowest hemolysis (0.39%), the lowest thrombus formation (40.36%), and the longest Partial Thromboplastin Time (PTT) (176 s). Overall, CAP demonstrated balanced performance, highlighting its potential for hemodialysis membrane development.

1. Introduction

Hemodialysis is a renal replacement therapy that removes metabolic waste products and excess body fluids, and maintains electrolyte balance in patients with kidney failure. The key component of this process is the hemodialysis membrane, which must possess semipermeable characteristics, high selectivity, and excellent biocompatibility to ensure efficient blood purification [1, 2, 3]. Currently, hemodialysis membranes are predominantly fabricated from synthetic polymers, such as polyacrylonitrile (PAN), polymethyl methacrylate (PMMA), and ethylene–vinyl alcohol (EVOH), which exhibit excellent separation performance but present environmental concerns due to their poor biodegradability [4, 5]. Therefore, the development of biodegradable membrane materials has emerged as a promising and more sustainable alternative.

Current research on hemodialysis membranes focuses on developing novel materials and structural modifications to enhance the selective removal of uremic toxins, particularly urea and creatinine, while minimizing the loss of essential proteins [3, 6, 7, 8]. Among the various approaches, the use of biopolymers such as cellulose, alginate, and especially chitosan has

attracted considerable attention due to their hydrophilicity, biocompatibility, biodegradability, non-toxicity, and environmental sustainability [4, 9]. Chitosan, a natural polysaccharide obtained through the deacetylation of chitin, contains reactive amino and hydroxyl groups that enable facile chemical modification through cross-linking or blending with other polymers to improve semipermeability, mechanical strength, and pH stability [10, 11, 12, 13]. These characteristics make chitosan a promising alternative to synthetic polymers for developing next-generation hemodialysis membranes with enhanced selectivity, hemocompatibility, and sustainability.

Previous studies have demonstrated that chitosan modification using various agents can significantly improve membrane properties for hemodialysis applications. Blending chitosan with polyethylene glycol (PEG) 4000 has been reported to enhance hydrophilicity, flexibility, mechanical strength, and pore homogeneity [14, 15, 16, 17]. In addition, cross-linking chitosan with short-chain dicarboxylic acids, such as malonic acid, malic acid, and adipic acid, has been shown to improve mechanical stability, increase hydrophilicity, and regulate pore size through interactions between the carboxyl groups of the cross-linkers and the amino groups of chitosan [18, 19, 20, 21, 22].

Furthermore, variations in the carbon chain length of dicarboxylic acids are expected to influence the cross-linked network architecture within the chitosan matrix, resulting in differences in cross-linking density, interchain spacing, pore structure, and free volume. The carbon chain length and molecular structure of dicarboxylic acids may influence chitosan chain spacing and network architecture. Malonic acid may introduce additional spacing between chitosan chains, while adipic acid may provide greater interchain separation due to its longer carbon chain [18, 22]. Malic acid, with its additional hydroxyl group (–OH) that may promote hydrogen bonding with chitosan and PEG 4000, is hypothesized to provide a balance between intermolecular interactions and network flexibility when combined with PEG 4000 and potentially enhance membrane performance for hemodialysis [19]. These structural variations are anticipated to affect the physicochemical properties, molecular transport behavior, and hemocompatibility of the membranes [20, 23].

Membrane thickness is another important parameter that influences the balance between solute clearance and mechanical stability in hemodialysis. Thinner membranes may facilitate solute transport by shortening diffusion pathways, but insufficient thickness may compromise mechanical integrity under operational stress [24, 25]. Conversely, thicker membranes may provide greater structural support while increasing resistance to solute diffusion. Therefore, membrane thickness must be optimized to balance transport performance and mechanical stability. However, previous studies have often focused on membrane composition or chemical modification, while the combined effects of different dicarboxylic acid crosslinkers and membrane thickness on the physicochemical properties, dialysis performance, and hemocompatibility of PEG 4000-blended chitosan membranes remain insufficiently understood. This highlights the need to investigate membrane thickness alongside crosslinker type to identify a suitable formulation for hemodialysis applications.

To address these research gaps, the primary objective of this study was to investigate how the carbon chain length of dicarboxylic acid cross-linkers (malonic, malic, and adipic acids) influences the physicochemical properties and performance relationships of chitosan-based hemodialysis membranes. PEG 4000 and the three dicarboxylic acids were incorporated into the chitosan matrix to investigate their effects on membrane composition and properties. Different casting volumes were also employed to investigate their effects on membrane thickness and pore structure.

The evaluation parameters in this study included membrane physical property measurements, physicochemical characterizations, mechanical properties, permeation performance using four permeates (urea, creatinine, vitamin B12, and bovine serum albumin (BSA)), and hemocompatibility. These evaluations were conducted to determine the effects of membrane composition and casting volume on the physicochemical properties, mechanical performance, separation characteristics, and blood compatibility of the membranes. The findings are expected to provide insights into the potential of these biodegradable chitosan-based membranes for hemodialysis applications and identify promising formulations for further optimization and evaluation under clinically relevant conditions.

2. Experimental

2.1. Materials

The materials used in this research were chitosan (Chimultiguna, Indonesia; Mw = 6.3×10^6 g/mol, degree of deacetylation (DD) = 89%), polyethylene glycol (PEG) 4000 (Merck; Mw = 4,000 g/mol), malonic acid (analytical grade; Sigma-Aldrich; 104.05 g/mol), malic acid (analytical grade; Merck; 134.09 g/mol), adipic acid (analytical grade; Merck; 146.14 g/mol), acetic acid (analytical grade; Merck; 60.05 g/mol), NaOH (Merck; 39.997 g/mol), creatinine (Merck; 113.11 g/mol), urea (Merck; 60.06 g/mol), vitamin B12 (Merck; Mw = 1355.37 g/mol), bovine serum albumin (BSA; HiMedia; Mw = 66.5 kDa), picric acid (Merck; 229.11 g/mol), *p*-dimethylaminobenzaldehyde (*p*-DMAB; Merck; 149.19 g/mol), HCl 37% (analytical grade; SmartLab), ethanol 96% (analytical grade; Merck), $NaH_2PO_4{\cdot}H_2O$ (Merck; 137.99 g/mol), Na_2HPO_4 (Merck; 141.96 g/mol), $CaCl_2$ (Merck; 110.99 g/mol), sodium dodecyl sulfate (SDS; Merck; 288.38 g/mol), glutaraldehyde 25% (analytical grade; Merck), NaCl (Merck; 58.44 g/mol), $CuSO_4{\cdot}5H_2O$ (Merck; 249.68 g/mol), and $KNaC_4H_4O_6{\cdot}4H_2O$ (Merck; 282.23 g/mol). Distilled water was obtained from the Integrated Laboratory of Diponegoro University. Human whole blood was used under ethical clearance No. 070/EC/KEPK/FK-UNDIP/VI/2026.

2.2. Preparation of Chitosan/Dicarboxylic Acid Solution

Crosslinked chitosan solutions were prepared by reacting a 1.5% (w/v) chitosan solution with malonic acid, malic acid, or adipic acid at a 1:1 molar ratio. The mixtures were stirred magnetically for 24 hours at room temperature and subsequently sonicated to remove air bubbles. The formulations obtained were labeled CS/O (malonic acid-crosslinked chitosan), CS/A (malic acid-crosslinked chitosan), and CS/D (adipic acid-crosslinked chitosan), corresponding to malonic acid, malic acid, and adipic acid, respectively.

2.3. Preparation of Chitosan/Dicarboxylic Acid/PEG 4000 Membranes

The overall molar ratio of chitosan, dicarboxylic acid, and PEG 4000 was maintained at 1:1:0.129. This ratio was obtained by normalizing the calculated molar amounts of the three components, initially expressed as 9.375:9.375:1.208, relative to the molar amount of chitosan. The molar amounts of chitosan and PEG were calculated based on the molar masses of their monomer units (160 g/mol for the monomer of chitosan and 62.07 g/mol for the monomer of PEG). The membranes were fabricated by the phase inversion method. The crosslinked chitosan solutions (CS/O, CS/A, and CS/D) were blended with PEG 4000 until homogeneous casting solutions were obtained. Each solution was cast onto Petri dishes at volumes of 5.0, 7.5, and 10.0 mL, followed by solvent evaporation at 40°C. The resulting films were coagulated in 2 M NaOH, washed with deionized water until neutral pH, and dried at room temperature. Five membrane formulations were prepared, namely CS, CP, COP, CAP, and CDP, as summarized in Table 1.

2.4. Characterization and Testing

2.4.1. Chemical Structure Characterization by FTIR

The chemical structure of the membranes was characterized using Fourier Transform Infrared (FTIR) spectroscopy. Spectra were collected over the range of 4000–400 cm^{-1} to identify functional groups and verify the blending and crosslinking of the membrane components.

Table 1. Composition of membrane variations

Membrane type	Chitosan (g)	Dicarboxylic acid			PEG 4000 (g)
		Malonic acid (g)	Malic acid (g)	Adipic acid (g)	
CS	1.5	0	0	0	0
CP	1.5	0	0	0	0.075
COP	1.5	0.975	0	0	0.075
CAP	1.5	0	1.25	0	0.075
CDP	1.5	0	0	1.36	0.075

2.4.2. Zeta Potential Characterization

The particle charge of the membrane solutions was analyzed using a Zetasizer Advanced Pro Blue Label. The membrane solutions were loaded into zeta potential capillary cells and analyzed at room temperature. Zeta potential was determined by the Electrophoretic Light Scattering (ELS) method, and electrophoretic mobility was converted into zeta potential using the Smoluchowski equation [26].

2.4.3. Surface Morphology Analysis by AFM

Surface morphology was characterized using atomic force microscopy (AFM) by scanning a 5 × 5 μm^2 area to evaluate surface topography and roughness. The roughness was quantified using the average roughness (Ra) and root mean square roughness (Rq) parameters.

2.4.4. Membrane Weight and Thickness Measurement

The weight and thickness of the membranes were measured before and after modification to evaluate changes resulting from the membrane preparation process. Membrane weight was determined using an OHAUS analytical balance, while thickness was measured with a Mitutoyo thickness meter.

2.4.5. Porosity

Membrane porosity was measured by immersing the membrane in 12 mL of distilled water for 24 hours. The membrane was then gently dried, and its weight was recorded before and after immersion to determine the dry and wet masses. Porosity was calculated using Equation 1.

$$\%Porosity = \frac{W_{wet}-W_{dry}}{V\times\rho_w} \times 100\% \quad (1)$$

Where V is the membrane volume (cm^3), and ρ_w is the density of water (1 g/cm^3).

2.4.6. Swelling Degree

The swelling degree of the membranes was determined by measuring the change in membrane diameter before (D_0) and after immersion in 12 mL of distilled water for 24 hours (D_s). The swelling percentage was calculated using Equation (2)

$$\%Swelling = \frac{D_s-D_0}{D_0} \times 100\% \quad (2)$$

2.4.7. Water Uptake

The membrane water uptake was determined by immersing the dry membrane in 12 mL of distilled water for 6 hours [27]. The membrane was periodically weighed after gentle drying to obtain the wet weight per hour (W_{wet}), and water uptake was calculated using Equation 3.

$$\%Water\ uptake = \frac{W_{wet}-W_{dry}}{W_{dry}} \times 100\% \quad (3)$$

2.4.8. Water Contact Angle

The water contact angle was measured using the sessile drop method to determine the membrane surface hydrophilicity. The contact angle image was captured and analyzed using Corel Draw software.

2.4.9. pH Resistance Test

The pH resistance of the membranes was evaluated by immersing them in 12 mL solutions with different pH values (3, 5, 7, 9, and 11) for 24 hours. The membrane weights before (W_0) and after immersion (W_t) were recorded to calculate the percentage weight change as an indicator of pH resistance (Equation 4).

$$\%Weight\ change = \frac{(W_t - W_0)}{W_t} \times 100\% \quad (4)$$

2.4.10. Biodegradable Test

The biodegradation of the membranes was evaluated by burying dry membrane samples in moist soil for 8 weeks or longer until no visible membrane residue remained. The membrane weight (W_t) was recorded weekly, and the degradation percentage was calculated from the initial and final weights (Equation 5).

$$\%Degree\ of\ degradation = \frac{W_t - W_0}{W_0} \times 100\% \quad (5)$$

2.4.11. Tensile Strength Test

Membranes (20 cm × 4 cm) were subjected to tensile testing in the wet state. The test was performed at a crosshead speed of 10 mm/min to determine the tensile strength (MPa) and elongation at break (%) of each membrane variation.

2.5. Transport Performance Test

The membrane permeability evaluation was conducted using a two-compartment dialysis chamber consisting of feed and receiving phases. The feed or donor phase was filled with individual permeate solutions of creatinine (2.5 mg/dL), urea (50 mg/dL), vitamin B12 (2.2 mg/dL), and BSA (480 mg/dL), while the receiving phase was filled with phosphate buffer solution (pH ~7.4). The dialysis process was carried out for 6 hours, with samples collected hourly from both compartments and analyzed by UV-Vis spectrophotometry at the following wavelengths: creatinine with picric acid at 483 nm; urea with *p*-DMAB at 420 nm; vitamin B12 at 367 nm; and BSA with Biuret reagent at 545 nm. The membrane with the best performance was further evaluated using a mixed permeate solution containing urea, creatinine, vitamin B12, and BSA simultaneously to assess its transport capability under more complex conditions.

2.6. Hemocompatibility Test

Blood compatibility of the membranes was evaluated by assessing protein adsorption, hemolysis ratio, partial thromboplastin time (PTT), and thrombus formation. In this study, Human whole blood (WB) was obtained from the researcher. Platelet-poor plasma (PPP) was prepared by centrifuging the whole blood at 3000 rpm for 15 minutes, followed by collection of the supernatant. This study was conducted in accordance with the relevant ethical requirements (Ethical Clearance No. 070/EC/KEPK/FK-UNDIP/VI/2026). Membrane samples were sterilized with 70% ethanol, soaked in PBS for 24 hours, and dried before testing. These parameters were used to evaluate the interaction between the membrane surface and blood components. Hemocompatibility tests, including protein adsorption, hemolysis, thrombus formation, and PTT, were performed according to ISO 10993-4:2017 [28].

2.6.1. Protein Adsorption Test

Protein adsorption was evaluated by immersing the membranes in PPP at 37°C for 60 minutes. After washing with PBS to remove unbound proteins, the adsorbed proteins were extracted using 2% SDS solution and quantified using the Biuret method. The absorbance was measured by UV-Vis spectrophotometry at 540–550 nm.

2.6.2. Hemolysis Ratio Test

The hemolytic activity of the membranes was determined by incubating membrane samples with diluted WB in 0.9% NaCl solution at 37°C for 60 minutes. The samples were centrifuged, and the absorbance of the supernatant was measured at 540 nm. The hemolysis ratio was calculated by comparison with positive (1% SDS) and negative (0.9% NaCl) controls.

2.6.3. Partial Thromboplastin Time (PTT) Test

The effect of membranes on blood coagulation was evaluated using the PTT test. Membranes were pre-incubated in PBS at 37°C, followed by exposure to PPP and $CaCl_2$ addition. The clotting time was determined by observing fibrin formation after incubation.

2.6.4. Thrombus Formation Test

Thrombus formation was evaluated by immersing membranes in whole blood at 37°C for 1 hour, followed by $CaCl_2$ addition and further incubation. The formed thrombi were washed, dried, and weighed to determine the thrombus mass.

3. Results and Discussion

3.1. Characterization and Test Results

The synthesis of chitosan-based dialysis membranes through blending and crosslinking with dicarboxylic acids and PEG was successfully achieved using the phase inversion method. The membrane-forming solutions exhibited good homogeneity, indicating proper dissolution and mixing of chitosan with the modifying agents. The formation of flexible and peelable membrane films after casting and drying further confirmed the successful membrane fabrication process. The incorporation of PEG and dicarboxylic acids was expected to influence the intermolecular interactions within the polymer matrix, leading to structural rearrangements that affect the physical and morphological characteristics of the resulting membranes.

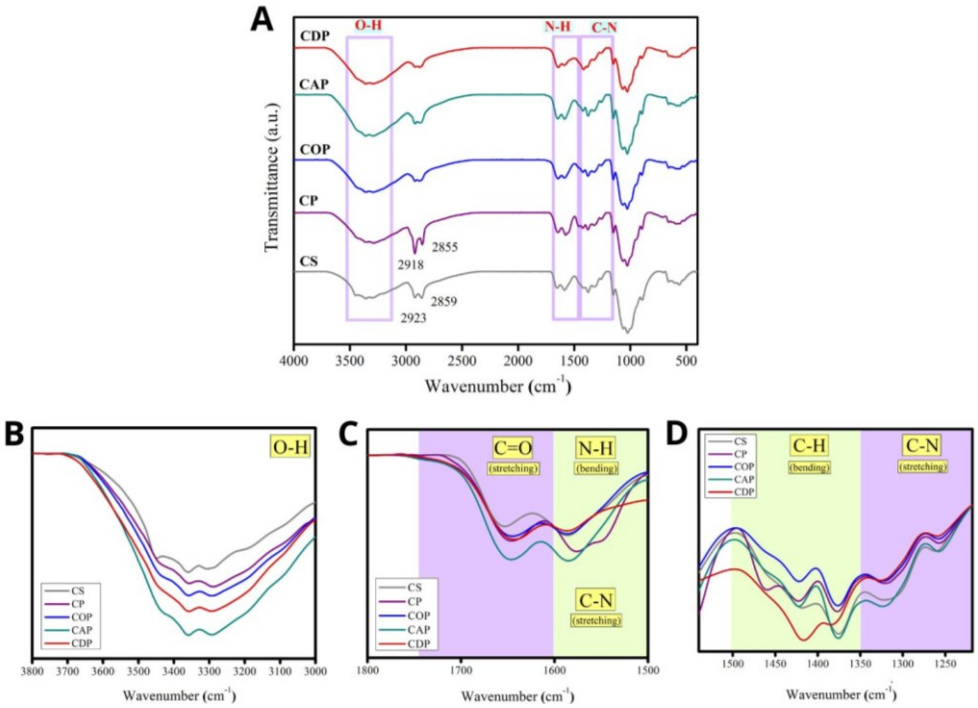


Figure 1. FTIR spectra of the five membrane variations: (A) Full spectra (4000–400 cm^{-1}), (B) O–H stretching region, (C) Carbonyl and amide region (1800–1500 cm^{-1}), and (D) C–H and C–N region (1550–1250 cm^{-1})

3.1.1. FTIR Spectra Analysis

As shown in Figure 1, the FTIR spectrum of the pure CS membrane exhibited characteristic absorption bands at 1653 cm^{-1} (amide I, C=O stretching), 1585 cm^{-1} (amide II, N–H bending), and 1377 cm^{-1} (C–H bending) [29]. After PEG 4000 incorporation, the O–H absorption band around 3360 cm^{-1} showed increased transmittance, indicating hydrogen bonding between CS and PEG (Figure 1(A)). In the crosslinked membranes (COP, CAP, and CDP), shifts in the bands near 1585 cm^{-1} and 1642–1646 cm^{-1} were observed, corresponding to protonated amine ($-NH_3^+$) and carboxylate ($-COO^-$) groups, confirming intermolecular interactions between chitosan and the dicarboxylic acids (Figure 1(C)) [18, 19, 21]. In addition, peak shifts and intensity changes were also observed in the regions of 1500–1350 cm^{-1} and 1350–1250 cm^{-1}, corresponding to CH_2 bending vibrations (and symmetric COO^- stretching) and C–N stretching vibrations (Figure 1(D)).

From the five membrane compositions, changes in the intensity of the O–H stretching band were also observed, as shown in Figure 1(B). The integrated peak area increased in the following order: CS < CP < COP < CDP < CAP. The increase in the integrated absorption peak area corresponds to greater infrared absorption, which is associated with decreased transmittance. This trend is consistent with the structural composition of the membranes, in which the incorporation of PEG increased the number of hydroxyl-containing groups, and a further enhancement was observed after crosslinking with dicarboxylic acids. Among the modified membranes, CAP exhibited the highest O–H band intensity, which can be attributed to the additional hydroxyl group present in malic acid.

Overall, the FTIR results indicate that membrane formation involved hydrogen bonding between CS and PEG, while crosslinking with malonic, malic, and adipic acids occurred through electrostatic interactions between protonated amine groups of chitosan and deprotonated carboxylate groups of the acids [30]. The proposed bonding interactions are illustrated in Figure 2. Based on their chemical structures, malonic acid is expected to provide the shortest spacing between crosslinked chitosan chains, followed by malic acid and adipic acid. This is attributed to differences in their molecular structures and the distance between their two carboxyl groups, which may influence the spacing between polymer chains when the acids act as crosslinking agents. However, FTIR analysis alone cannot establish differences in network density. Therefore, the implications of these structural differences should be considered alongside the swelling behavior, which reflects changes in membrane dimensions upon immersion.

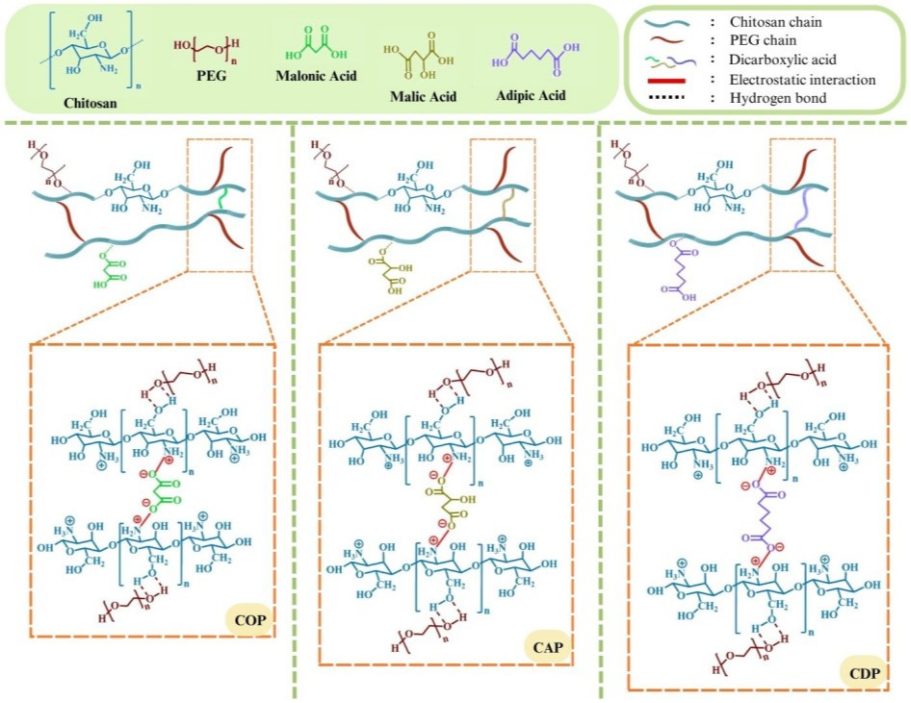


Figure 2. Schematic illustration of the proposed interactions between chitosan, PEG 4000, and dicarboxylic acids

3.1.2. Zeta Potential

The results of zeta potential measurements, as shown in Figure 3, show that all membranes have a positive charge with values ranging from +55.8 to +74.58 mV. The CS membrane exhibits a zeta potential of +58.91 mV, arising from the protonation of chitosan amino groups. The addition of PEG causes a slight decrease to +55.8 mV because PEG is non-ionic and can cover some of the amino groups on the membrane surface. In contrast, dicarboxylic acid cross-linking increased the zeta potential to +72.68 mV (COP), +67.21 mV (CAP), and +74.58 mV (CDP), indicating structural reorganization that enhanced the exposure of protonated amino groups.

The highest zeta potential value was obtained on the CDP membrane. This phenomenon may be attributed to the longer carbon chain of adipic acid compared with malonic and malic acids, which increases the distance between polymer chains and may prevent some chitosan amino groups from participating directly in cross-linking interactions [31]. As a result, some amino groups remain available for protonation to form $-NH_3^+$ groups, thereby contributing to the increase in the measured positive charge. The zeta potential results did not follow the same trend as the measured pH values, indicating that the differences in zeta potential may not be attributed to pH alone, but may also be influenced by other factors, such as ionic strength and interactions among the components of the membrane-forming solutions.

The effect of surface charge on urea and creatinine transport was not expected to be significant. This is because urea is a neutral molecule, whereas creatinine is only weakly charged in solution. CDP membranes have the highest positive charge density, thus potentially having the strongest electrostatic interactions with negatively charged species, such as protein molecules. The higher the positive surface charge, the stronger the possibility of electrostatic interactions with negatively charged protein [32]. Consequently, protein adsorption on the membrane surface can increase if other factors such as hydrophilicity and surface roughness are unable to inhibit the process.

3.1.3. Surface Morphology Analysis by AFM

Based on the AFM analysis (Figures 4 and Table 2), the membrane surface roughness increased in the order of COP < CS < CP < CDP < CAP. COP exhibited the lowest Ra, Rq, and Rz values, indicating the smoothest surface due to a more homogeneous polymer distribution and a more uniform crosslinked network. In contrast, the incorporation of PEG increased the surface roughness of the CS membrane, likely because of phase separation and the formation of more heterogeneous polymer domains.

Among the crosslinked membranes, CAP showed the highest average roughness (Ra and Rq), which may be attributed to the additional hydroxyl group of malic acid that enhances hydrogen bonding, promoting local polymer aggregation during solvent evaporation and membrane drying, thereby producing a rougher surface morphology in the dried membrane [33]. Meanwhile, CDP exhibited the highest Rz value, indicating greater differences between the highest peaks and deepest valleys, reflecting more pronounced local surface irregularities. Interestingly, this trend differed from the zeta potential results, in which CDP exhibited the most positive surface charge. This finding suggests that protein adsorption was influenced not only by the electrostatic properties of the membrane but also by its surface morphology.

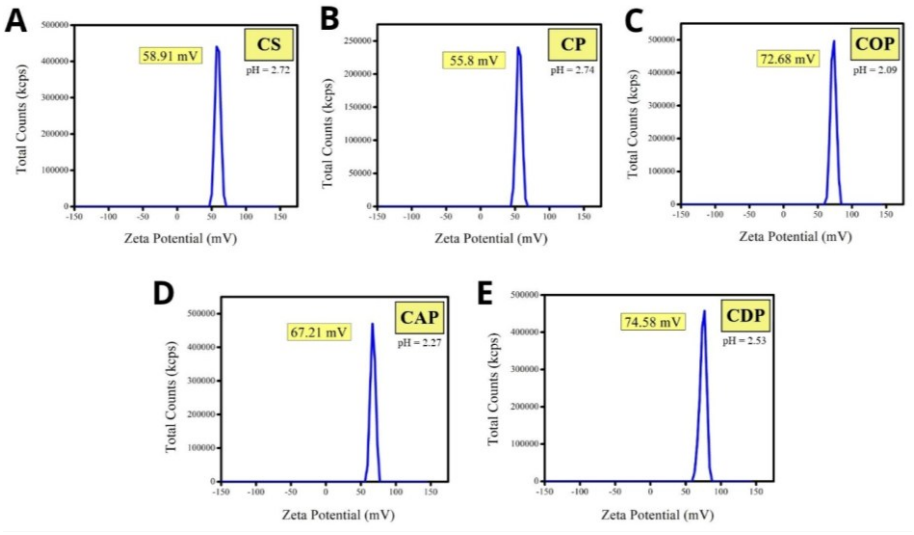


Figure 3. Results of zeta potential test of membrane solutions after tenfold dilution (A) CS, (B) CP, (C) COP, (D) CAP, and (E) CDP

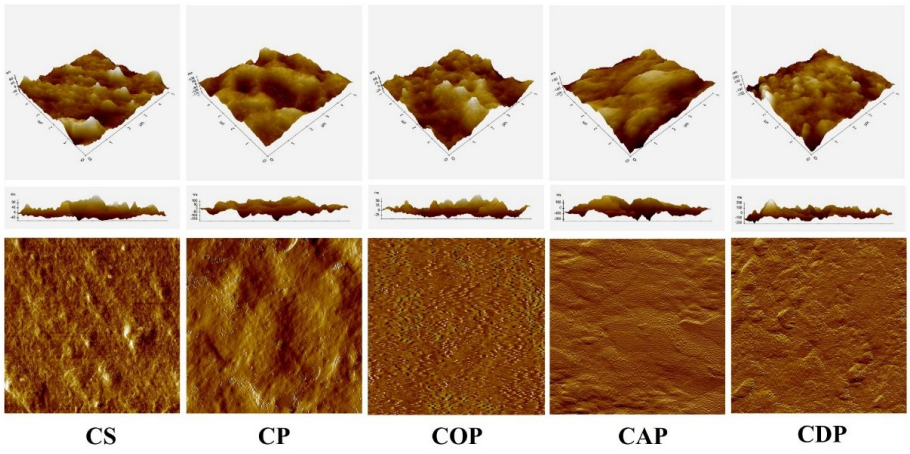


Figure 4. AFM surface topography images of the fabricated membranes obtained over a scan area of 5 × 5 μm²

Table 2. AFM-derived surface roughness parameters of the five membrane variations

Parameter of roughness	CS	CP	COP	CAP	CDP
Rq	22.34	46.26	17.17	59.39	51.31
Ra	16.85	37.96	13.61	46.38	39.17
Rz	168.43	292.43	112.76	364.13	406.18

3.1.4. Weight and Thickness

In Table 3, the membrane weight and thickness varied with the crosslinking agent and casting volume. The incorporation of PEG 4000 increased the membrane weight relative to pure chitosan, whereas crosslinking with dicarboxylic acids initially reduced it, likely due to the additional solvent used during membrane preparation. Among the crosslinked membranes, the weight increased with the molecular weight of the dicarboxylic acid, following the order COP < CAP < CDP. Increasing the casting volume from 5 to 7.5 and 10 mL also resulted in higher membrane weights for all formulations.

Table 3. Results of the weight and thickness of the membrane

Type of membrane	Weight (×10¹ mg)			Thickness (×10⁻² mm)		
	5 mL	7.5 mL	10 mL	5 mL	7.5 mL	10 mL
CS	7.02	10.72	13.05	6.40	7.60	8.40
CP	7.20	10.87	14.28	6.80	7.20	7.80
COP	4.77	7.23	9.22	6.20	7.60	7.80
CAP	4.80	7.28	10.10	8.00	8.40	11.00
CDP	4.81	7.57	10.26	7.60	8.20	11.60

The average wet membrane thickness at a casting volume of 5 mL increased in the order COP < CS < CP < CDP < CAP. Although the crosslinked solutions (COP, CDP, and CAP) appeared less viscous than the CS and CP solutions, the resulting membrane thicknesses were also influenced by the final membrane diameter. In particular, CAP and CDP exhibited smaller diameters in both the dry and wet states, resulting in greater thicknesses than CS and CP. In contrast, COP exhibited a larger diameter than CAP and CDP, corresponding to a lower thickness. As with membrane weight, thickness increased with increasing casting volume across all membrane variations.

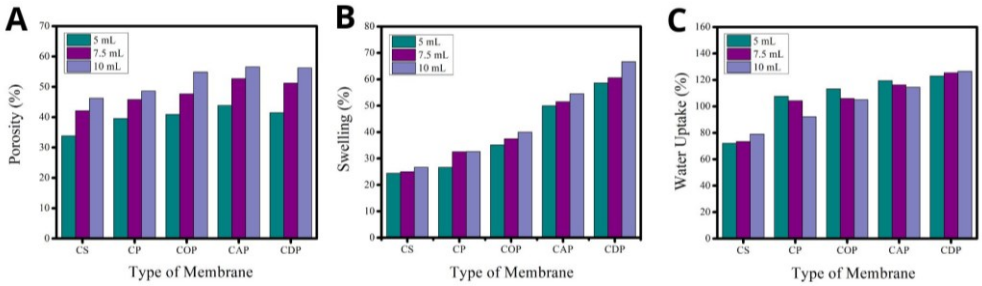


Figure 5. (A) Porosity, (B) Swelling degree, and (C) Water uptake

Furthermore, the CS and CP membranes exhibited different trends in weight and thickness at casting volumes of 7.5 and 10 mL. At casting volumes of 7.5 and 10 mL, the CP membranes exhibited larger diameters than the corresponding CS membranes and were therefore not necessarily thicker than CS. This observation suggests that the additional casting solution may have promoted greater lateral spreading of CP rather than a proportional increase in thickness. Therefore, membrane thickness depends not only on membrane weight but also on the extent of lateral spreading and the resulting membrane geometry.

3.1.5. Porosity Test

The porosity test, conducted by immersing the membranes in distilled water for 24 hours, revealed variations in porosity among the membrane formulations, which may be influenced by material composition and fabrication conditions. Porosity reflects the formation of a porous structure that plays an important role in membrane transport properties. As shown in Figure 5(A), at a casting volume of 5 mL, the CS membrane exhibited the lowest porosity (33.85%), whereas the CAP membrane exhibited the highest porosity (43.85%), followed by the CDP membrane (41.46%). The relatively high porosity of CAP may be associated with the incorporation of malic acid as a crosslinking agent. Malic acid contains both carboxyl groups (-COOH) and a hydroxyl group (-OH), which may contribute to the hydrophilicity of the polymer network and facilitate water penetration into the membrane structure [19]. Meanwhile, the relatively high porosity of CDP may be related to the longer aliphatic carbon chain of adipic acid, which may influence the arrangement and spacing of polymer chains, potentially promoting the formation of a more open membrane structure [21, 33]. Furthermore, increasing the membrane casting volume from 5 mL to 7.5 mL and 10 mL led to a corresponding increase in porosity for all membrane types.

The increase in porosity at higher casting thicknesses may be associated with the combined effects of membrane thickness and the chemical structure of the crosslinking agents used. Increasing the casting volume may influence the formation of the membrane's internal structure, including the distribution of voids and pore channels accessible to water. Meanwhile, malic acid, used as the crosslinking agent in the CAP membrane, contains hydroxyl (-OH) groups that may enhance the hydrophilicity of the polymer network [19]. The increased hydrophilicity may facilitate water penetration and retention within the membrane matrix during 24 hours of immersion, potentially contributing to CAP exhibiting the highest apparent porosity among all tested membrane formulations. These findings suggest that membrane porosity is influenced not only by casting thickness and the carbon chain length of the crosslinking agent but also by the availability of hydrophilic functional groups and the internal structure of the resulting polymer matrix.

3.1.6. Swelling Degree Test

The degree of swelling analysis revealed variations in the dimensional changes of the membranes, as determined by changes in membrane diameter after 24 hours of immersion in distilled water. As shown in Figure 5(B), the swelling behavior did not completely follow the porosity trend, indicating that membrane expansion was not determined by porosity alone. Differences in the chemical structures of the dicarboxylic acid crosslinkers may also contribute to the observed swelling behavior. As illustrated by the proposed molecular structures in Figure 3, COP has the shortest carbon chain, followed by CAP, which contains an additional hydroxyl group, and CDP, which has the longest aliphatic chain. These structural differences may influence the arrangement of the chitosan network and, consequently, the extent of dimensional expansion upon immersion.

Furthermore, the degree of swelling increased with casting volume, indicating greater diameter expansion after immersion. Among all samples, the CDP membrane exhibited the highest degree of swelling (58.62, 60.60, and 66.66%), followed by CAP and COP. These findings suggest that membranes crosslinked with dicarboxylic acids developed a more interconnected porous network, which facilitated greater water penetration and retention within the polymer matrix during the 24-hour immersion period. Consequently, the enhanced pore interconnectivity and increased free volume contributed to the superior swelling behavior observed in these membranes.

3.1.7. Water Uptake

The water uptake results differed slightly from the porosity and degree of swelling measurements. At a casting volume of 5 mL, the water uptake exhibited the same trend as the previous two tests. However, at higher casting volumes (7.5 and 10 mL), the water uptake behavior varied among the five membrane compositions, indicating differences in their water absorption kinetics. An increase in water uptake was observed for the CS and CDP membranes, whereas the CP, COP, and CAP membranes exhibited a decrease. Nevertheless, the CDP

membrane consistently exhibited the highest overall water uptake (123.05, 125.36, and 126.48%) at casting volumes of 5, 7.5, and 10 mL. These results in Figure 5(C) suggest that the increase in water uptake with increasing casting volume observed for CS and CDP may be associated with differences in water absorption capacity, the accessibility of the internal membrane structure, and interactions between water and the polymer matrix. In CS, the hydroxyl and amino groups of chitosan can interact with water, whereas in CDP, interactions between chitosan and adipic acid may influence the polymer chain arrangement and water retention [21]. In contrast, CP, COP, and CAP exhibited decreasing water uptake as casting volume increased, suggesting that their short-term water absorption behavior may be influenced by composition-dependent changes in membrane structure and water accessibility.

Notably, porosity increased with increasing casting volume across all membrane formulations after 24 hours of immersion. This finding, together with the different water uptake trends observed after 6 hours, suggests that water absorption during the 6-hour test may not have reached its maximum under the tested conditions. Thus, the water uptake measured at 6 hours may reflect differences in short-term water absorption behavior rather than the maximum water-holding capacity of the membranes. However, further measurements at multiple immersion times would be required to confirm whether water uptake had reached equilibrium [34].

3.1.8. Water Contact Angle

The water contact angle results, as shown in Table 4, differed from those obtained in the previous characterization tests. Unlike porosity, swelling degree, and water uptake measurements, the water contact angle test evaluates the wettability of the membrane surface immediately upon contact with a water droplet, without requiring water to penetrate or be absorbed into the membrane matrix. Consequently, this analysis primarily reflects the surface hydrophilicity rather than the bulk water absorption behavior of the membrane. Among the tested membranes, the CAP membrane exhibited the lowest water contact angle, indicating the highest surface hydrophilicity, whereas the CS membrane showed the highest contact angle, corresponding to the lowest wettability and hydrophilicity among the tested membranes.

The superior hydrophilicity of the CAP membrane can be attributed to the incorporation of malic acid, which contains two carboxyl (–COOH) groups and an additional hydroxyl (–OH) group. The presence of the extra hydroxyl group provides additional hydrogen-bonding sites, thereby enhancing the affinity of the membrane surface toward water [10, 35]. The COP membrane, crosslinked with malonic acid, exhibited the second-highest hydrophilicity because malonic acid has two carboxyl groups and a relatively short carbon chain, yielding a highly polar crosslinking structure. In contrast, the CDP membrane crosslinked with adipic acid exhibited lower hydrophilicity than CAP and COP despite containing two carboxyl groups. This may be related to the longer aliphatic chain of adipic acid compared with malic and malonic acids [21]. The longer hydrocarbon segment may increase the relative nonpolar character of the crosslinked network, thereby reducing its affinity for water despite the presence of carboxyl groups [10, 35].

3.1.9. pH Resistance Performance

Based on Figure 6, the pH resistance test demonstrated the stability of each membrane across pH levels (3, 5, 7, 9, and 11). At pH 3, all membrane variations exhibited 100% weight loss, indicating complete structural degradation under strongly acidic conditions. This is attributed to the protonation of chitosan amino groups, which disrupts intermolecular interactions and weakens the polymer network, leading to membrane dissolution. At pH 5, some membranes still exhibited weight loss, suggesting partial destabilization of the polymer structure under mildly acidic conditions.

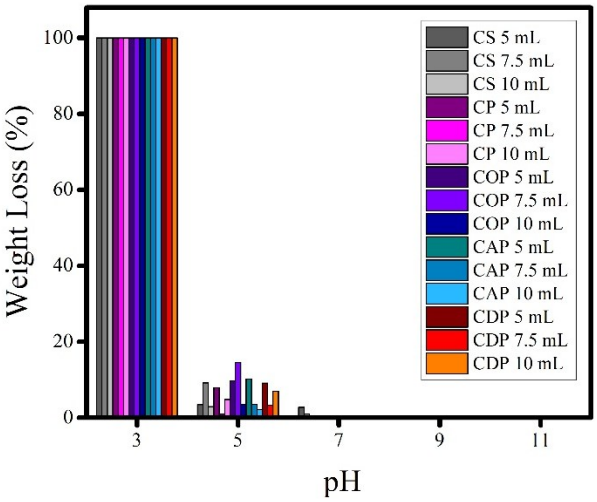
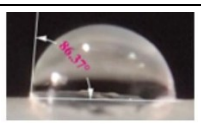
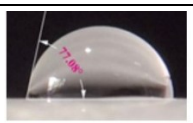
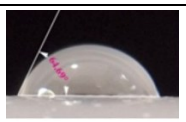
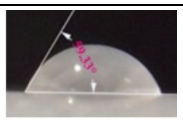
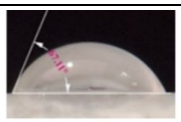


Figure 6. pH stability of the fabricated membrane variations

Table 4. Water contact angle

Type of membrane	CS	CP	COP	CAP	CDP
Droplet image					
Contact angle	86.37°	77.08°	64.69°	59.33°	67.11°

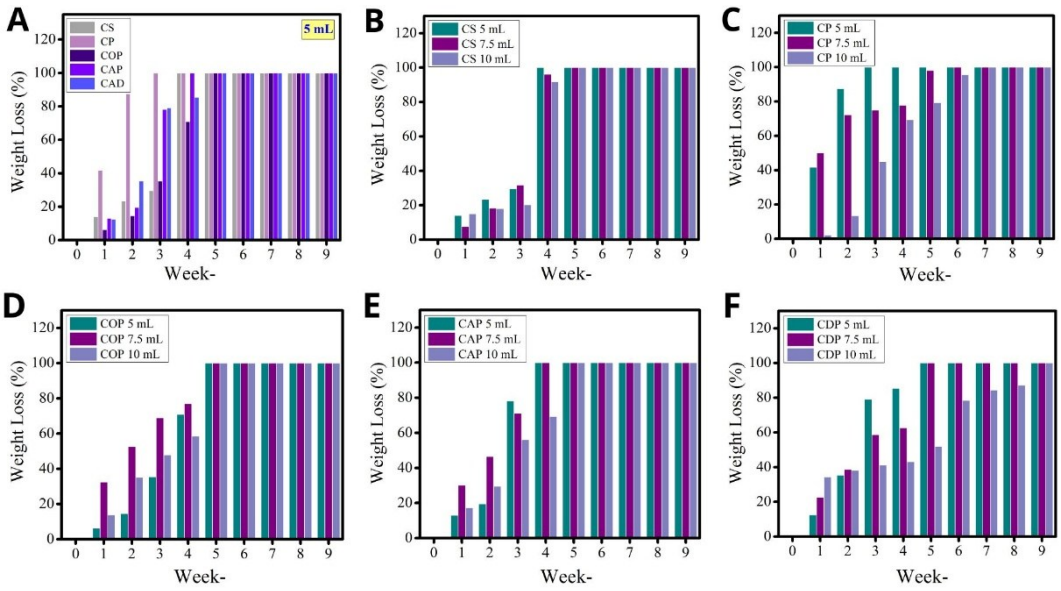


Figure 7. Biodegradation behavior of the fabricated membrane variations: (a) each variation on casting volume of 5 mL, (B) CS, (C) CP, (D) COP, (E) CAP, and (F) CDP

At pH 7, only the unmodified CS membrane exhibited weight loss (2.70% for 5 mL and 1.02% for 7.5 mL), while the crosslinked membranes remained stable. The improved stability of the modified membranes was attributed to the stronger polymer network formed by dicarboxylic acid crosslinking, which limited chain mobility and prevented dissolution. This stability at neutral pH is crucial for hemodialysis applications, as it closely matches the physiological blood pH (~7.4) [36, 37]. Under alkaline conditions (pH 9 and 11), all membranes remained intact, a result attributed to the low solubility of chitosan.

3.1.10. Biodegradation Performance

The biodegradation test revealed different degradation behaviors among the membrane variations within 9 weeks. Based on composition (Figure 7(A)), the degradation rate at a casting volume of 5 mL followed the order CP > CAP > COP > CDP > CS. The CP membrane exhibited the fastest degradation due to PEG incorporation, which increased membrane hydrophilicity and free volume, facilitating water penetration and polymer degradation [38]. The dicarboxylic acid-crosslinked membranes showed slower degradation due to the formation of a more stable network. Among them, CAP degraded faster than COP and CDP because the hydroxyl (-OH) group of malic acid enhanced hydrophilicity and water accessibility, whereas CDP showed the lowest degradation rate due to the longer carbon chain of adipic acid, which reduced membrane polarity and limited water penetration [20].

Based on membrane thickness, thinner membranes generally degraded faster due to lower polymer mass and shorter water diffusion pathways (Figure 7(B, C, and F)). However, this trend was not observed for COP and CAP (Figure 7(D and E)), likely due to the higher contribution of hydrophilic functional groups from the crosslinkers in thicker membranes. The increased presence of malonic and malic acid facilitated water penetration and hydrolytic degradation, particularly in CAP due to its additional hydroxyl (−OH) group. Therefore, biodegradation behavior was influenced not only by membrane thickness but also by the balance between crosslinking structure, hydrophilicity, and water accessibility within the polymer matrix.

3.1.11. Tensile Strength

Tensile strength tests were conducted on wet membranes to better represent hemodialysis conditions, where membranes are exposed to an aqueous environment and come into contact with blood. This wet state provides a more relevant assessment of their mechanical behavior under conditions closer to their intended application. The mechanical properties of the membranes, evaluated through tensile strength and elongation in Table 5, were influenced by membrane composition and casting volume. The lowest tensile strength was observed for the COP membrane at 5 mL and 10 mL, while the highest was obtained for the CP membrane at the same volumes. The lower tensile strength of COP may be related to the shorter carbon chain of malonic acid, which provides weaker reinforcement within the chitosan network [39]. In contrast, the CP membrane exhibited the highest tensile strength at both casting volumes, potentially due to PEG–chitosan interactions that influence intermolecular cohesion and stress transfer, resulting in higher tensile strength.

Table 5. Results of membrane tensile strength test

Membrane	Tensile stress (MPa)		Elongation (%)	
	5 mL	10 mL	5 mL	10 mL
CS	0.38	1.43	14.62	29.80
CP	0.94	2.97	16.45	24.90
COP	0.17	1.12	12.39	51.49
CAP	0.78	1.32	29.53	46.95
CDP	0.6	1.09	23.65	33.84

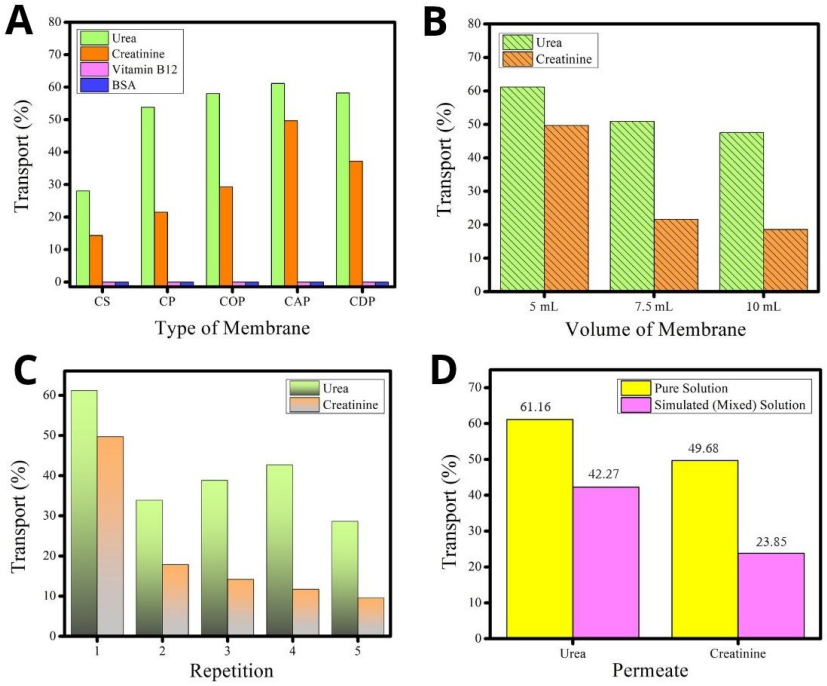


Figure 8. Transport performance of: (A) Urea, creatinine, vitamin B12, and albumin on 5 mL membranes, (B) CAP membrane on different casting volumes, (C) Repetition on CAP membrane, and (D) CAP membrane on different solutions

The elongation results showed a different trend overall, although the membranes cast at 5 mL followed the same order as the wet membrane thickness results (Table 3) at the same casting volume (COP < CS < CP < CDP < CAP). The COP membrane at 5 mL and CP membrane at 10 mL exhibited the lowest elongation. The CP membrane had lower elongation at break than the CS membrane at 10 mL, which may be associated with its higher porosity, as pores can act as stress concentration sites and restrict deformation under wet conditions. While CAP at 5 mL and COP at 10 mL showed the highest elongation. The higher elongation of CAP was attributed to the hydroxyl (−OH) group of malic acid, which increased hydrophilicity and chain mobility. Meanwhile, the increased elongation of COP at 10 mL may result from greater water accessibility and membrane thickness, which promoted polymer chain movement [29, 40]. Overall, the mechanical behavior was governed by the balance between crosslinking structure. polymer interactions. and membrane flexibility.

3.2. Permeation Performance in Dialysis

The membrane permeation performance was evaluated through four transport tests, as shown in Figure 8. Based on Figure 8(A), the transport of four model solutes (urea, creatinine, vitamin B12, and BSA) was investigated using membranes prepared at the lowest casting volume (5 mL) to evaluate the rejection of larger solutes while maintaining the transport of small uremic toxins. All membrane variations completely rejected vitamin B12 and BSA, indicating that the membrane pore sizes were smaller than the molecular dimensions of these macromolecules [41, 42]. The high rejection of BSA and vitamin B12 demonstrates the membrane's ability to retain relatively large molecules and may contribute to its selective transport characteristics. While BSA represents a large protein, vitamin B12 is an essential nutrient that should be maintained at adequate levels in patients undergoing hemodialysis [43, 44]. Therefore, the retention of these solutes may help minimize the loss of essential biological components during dialysis. However, this selectivity must be balanced with effective clearance of uremic toxins. In contrast, urea and creatinine readily permeated the membranes due to their significantly smaller molecular sizes [45].

Among the tested membranes, the CAP membrane exhibited the highest transport efficiencies for urea (61.16%) and creatinine (49.68%), followed by CDP, COP, CP, and CS (28.06% for urea and 14.34% for creatinine). The superior transport performance of CAP is attributed to the use of malic acid as the crosslinking agent. In addition to its two carboxyl groups, malic acid contains an additional −OH group that increases membrane hydrophilicity and promotes the formation of a hydrated transport pathway, facilitating the diffusion of small solutes. The CDP membrane exhibited the second-highest transport due to the longer carbon chain of adipic acid, which increased free volume within the polymer matrix, although its lower hydrophilicity than malic acid limited solute diffusion. Meanwhile, the COP membrane exhibited moderate transport performance because malonic acid possesses a shorter carbon chain and lacks the additional −OH group, resulting in lower free volume and hydrophilicity than CAP. These results suggest that membrane transport is governed not only by pore size but also by the hydrophilicity and molecular structure of the crosslinking agent, which together regulate water-mediated diffusion through the membrane.

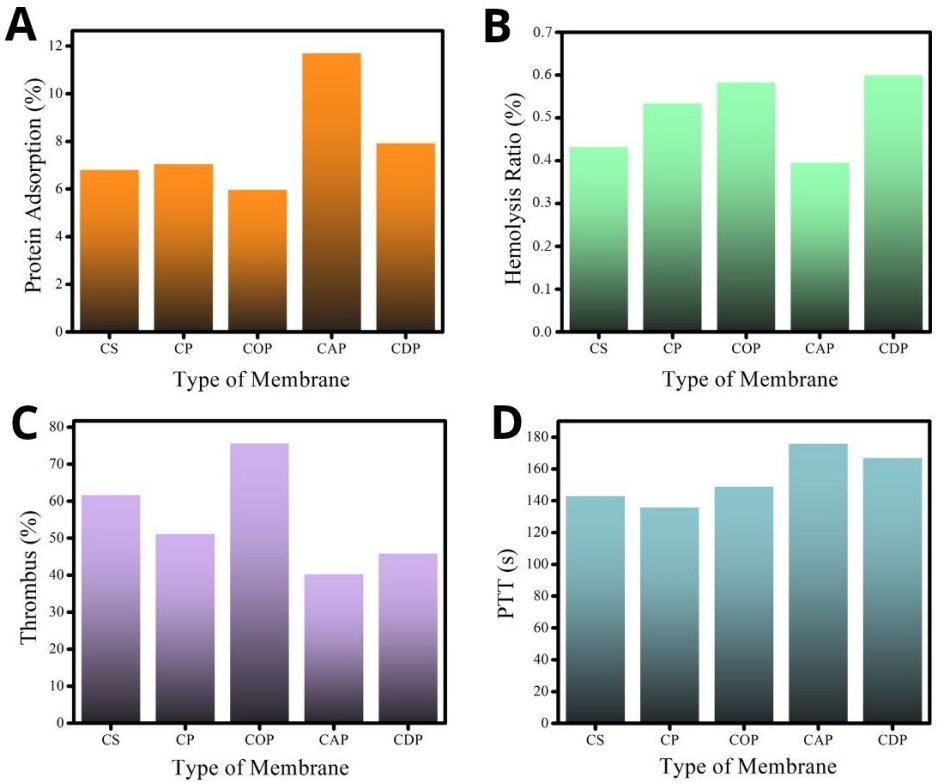


Figure 9. Hemocompatibility behavior of the fabricated membrane variations on: (A) Protein adsorption, (B) Hemolysis ratio, (C) Thrombus formation, and (D) PTT

As shown in Figure 8(B), the transport performance of the CAP membrane, which exhibited the best overall permeation performance, was further evaluated at different casting volumes (5, 7.5, and 10 mL) to investigate the effect of membrane thickness. Only urea and creatinine were used as permeating solutes because of their relatively small molecular sizes. The results showed that the 5 mL membrane achieved the highest transport efficiencies for both urea and creatinine, followed by the 7.5 mL and 10 mL membranes. This trend is primarily attributed to the increase in membrane thickness as casting volume increases. Thicker membranes provide a longer diffusion pathway and greater transport resistance, thereby reducing the diffusion rate of small solutes across the membrane. Although increasing the casting volume also increased membrane porosity, the effect of the longer diffusion distance was more dominant, resulting in lower overall permeation [46, 47]. These findings indicate that membrane thickness plays a critical role in determining transport performance, with thinner membranes offering more efficient diffusion while maintaining sufficient selectivity.

After identifying the 5 mL CAP membrane as the optimal composition, its transport performance was further evaluated through five consecutive dialysis cycles using urea and creatinine as model solutes (Figure 8(C)). The transport efficiency of both solutes gradually decreased with repeated use, indicating progressive membrane fouling and reduced mass transfer efficiency. The decline was more pronounced for creatinine, whereas urea transport remained relatively stable, showing only a slight fluctuation with a temporary increase during the fourth cycle before decreasing again in the fifth cycle. This difference is likely attributed to the smaller molecular size and higher diffusion coefficient of urea, which allow it to diffuse through the membrane more readily even after partial pore blockage. In contrast, creatinine, with a larger molecular size and lower diffusivity than urea, is more susceptible to transport resistance due to pore fouling or partial blockage during repeated dialysis cycles. These results indicate that the membrane exhibits its highest dialysis performance during the initial cycle, while repeated use progressively reduces transport efficiency due to membrane fouling [48, 49]. Therefore, membrane regeneration or replacement should be considered to maintain optimal dialysis performance in practical applications.

The final transport test compared the performance of the 5 mL CAP membrane using single-solute and mixed-solute systems (Figure 8(D)). The single-solute system, containing either urea or creatinine alone, was used to determine the maximum transport efficiency of each solute. In contrast, the mixed-solute system, consisting of urea, creatinine, vitamin B12, and BSA, was designed to simulate a more realistic hemodialysis environment in which small uremic toxins coexist with larger biomolecules. The results showed that the transport efficiency of urea decreased from 61.16% to 42.27%, while creatinine transport decreased more markedly from 49.68% to 23.85% in the mixed-solute system. This reduction indicates that the presence of larger molecules hindered the diffusion of small solutes through the membrane. Although vitamin B12 and BSA were completely rejected due to their larger molecular sizes, their accumulation near the membrane surface likely

caused concentration polarization and partial pore blockage, thereby increasing mass-transfer resistance. BSA can induce membrane fouling through adsorption on the membrane surface and protein cake layer formation, while vitamin B12 may contribute to fouling through adsorption or interactions with membrane pores.

The positively charged membrane surface, as indicated by the zeta potential results (Figure 3), may promote electrostatic attraction with negatively charged BSA under the experimental conditions, facilitating protein adsorption and subsequent cake layer formation [32]. This protein layer can increase mass-transfer resistance and reduce the diffusion of urea and creatinine. In contrast, vitamin B12, which has a relatively large molecular structure, may contribute to transport resistance through steric hindrance, pore restriction, or adsorption, depending on the membrane pore size and surface chemistry [50, 51].

Therefore, the reduction in urea and creatinine diffusion is more likely associated with BSA and vitamin B12 fouling. Furthermore, competition among solutes for available transport pathways reduced the effective diffusion of urea and creatinine [52]. The greater reduction observed for creatinine is likely due to its lower diffusion coefficient and larger molecular size than urea, making its transport more sensitive to the increased diffusion resistance. These findings suggest that membrane performance evaluated using mixed-solute systems provides a more realistic assessment of dialysis performance than single-solute experiments, as it better represents the competitive transport conditions encountered during hemodialysis.

3.3. Hemocompatibility Test

The hemocompatibility of the membranes was evaluated through four assays, namely protein adsorption, hemolysis ratio, thrombus formation, and PTT, using membranes prepared at a casting volume of 5 mL as shown in Figure 9. In the protein adsorption test (Figure 9(A)), the CAP membrane exhibited the highest protein adsorption, whereas the COP membrane showed the lowest. The lower protein adsorption of the COP membrane indicates a reduced affinity for plasma proteins, while the higher adsorption observed for CAP is likely associated with its greater surface hydrophilicity and the presence of additional –OH groups that promote protein–surface interactions [53, 54]. Furthermore, the protein adsorption trend was more consistent with the surface roughness measured by AFM (Table 2) than with the zeta potential results (Figure 3), suggesting that surface morphology played a more dominant role than surface charge in governing protein adsorption under the present experimental conditions. Membranes with higher surface roughness provided a larger effective surface area and more favorable sites for protein attachment.

Based on Figure 9(B), the hemolysis assay results showed that the COP membrane produced the higher value, because of the highest erythrocyte damage, while CAP membrane produced the lowest value (0.39%), indicating that CAP possessed the best blood compatibility with minimal erythrocyte damage [55]. But all tested membranes still exhibited very minor damage, as hemolysis rates were less than 0.6% and the materials were considered non-hemolytic based on ASTM F756 and ISO 10993-4 [28, 56]. A similar trend was observed in the thrombus formation test as shown in Figure 9(C), where the COP membrane generated the greatest amount of thrombus, while CAP exhibited the least thrombus formation (40.36%), demonstrating its lower thrombogenicity and reduced tendency to activate blood coagulation [1].

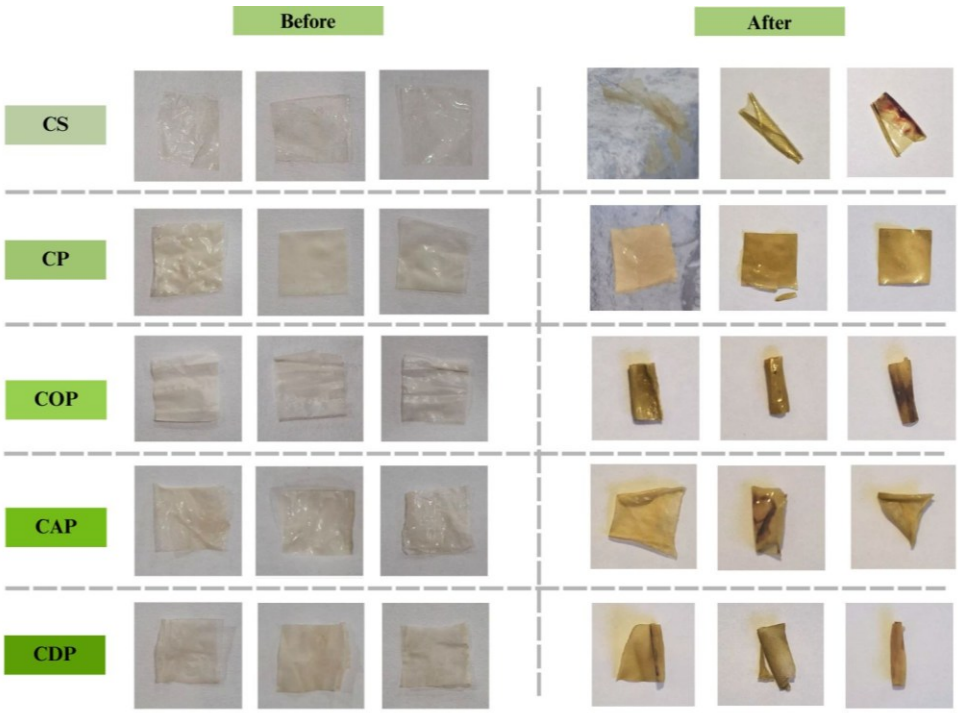


Figure 10. Membrane appearance before and after the thrombus formation test

Visual comparison of the membrane surfaces before and after the thrombus formation test is shown in Figure 10. As shown in Figure 10, visible blood deposits were observed on the COP membrane, potentially reflecting the retention of blood components on its surface and contributing to the observed thrombus accumulation. Consistent with those findings, the PTT assay, as shown in Figure 9(D), revealed that the CP membrane induced the fastest clot formation (136 seconds), whereas the CAP membrane exhibited the longest clotting time (176 seconds). A prolonged PTT indicates delayed activation of the intrinsic coagulation pathway, suggesting that the CAP membrane possesses superior anticoagulant properties [57]. The increased hydrophilicity of the CAP membrane may promote the formation of a stable hydration layer on its surface, thereby potentially limiting the activation of surface-induced coagulation [58]. The CP membrane exhibited the fastest clot formation after the CS membrane, which may be associated with changes in surface chemistry following the incorporation of synthetic PEG into the chitosan-dense matrix. If PEG coverage is incomplete or nonuniform, exposed chitosan-rich regions may interact with plasma proteins, potentially promoting contact-mediated coagulation.

Overall, the CAP membrane demonstrated favorable hemocompatibility compared with all other tested membranes, as indicated by its low hemolytic activity, minimal thrombus formation, and prolonged PTT (coagulation kinetics at first contact), even with the highest protein adsorption. This is because the total protein adsorption assay measures multiple plasma proteins, not only fibrinogen, which plays an important role in clot (thrombus) formation [59, 60, 61]. Therefore, high total protein adsorption does not necessarily indicate high fibrinogen formation as the result of thrombus formation, which is consistent with the minimal thrombus formation observed for the CAP membrane. Although the CAP membrane exhibited the highest protein adsorption, it still showed overall favorable performance across permeation, selectivity, and other hemocompatibility parameters. This suggests that the CAP membrane, especially CAP 5 mL, warrants further investigation for potential applications in hemodialysis.

4. Conclusion

The incorporation of PEG 4000 and dicarboxylic acid cross-linkers modified the physicochemical properties of the chitosan-based membranes. FTIR analysis revealed broadening of the O–H stretching band (typically around 3200–3600 cm^{-1}) and shifts in the C=O stretching band (approximately 1750–1600 cm^{-1}), N–H bending (approximately 1650–1500 cm^{-1}), and C–N stretching band (approximately 1550–1250 cm^{-1}), suggesting changes in the chemical interactions within the membrane matrix. Zeta potential measurements showed that all membranes maintained positive surface charges (from +55.80 mV to +74.58 mV). AFM analysis revealed differences in surface morphology, with CAP exhibiting the highest surface roughness (Rq = 59.39 nm and Ra = 46.38 nm). Membrane modification increased porosity, degree of swelling, water uptake, and thickness. CAP exhibited the highest hydrophilicity, with a water contact angle of 59.33°. Most membranes remained stable at pH 7–11 and completely degraded after 9 weeks. Regarding mechanical properties, CP exhibited the highest tensile strength, with reported values of 0.94 and 2.97 MPa, whereas CAP at 5 mL and COP at 10 mL showed the highest elongation at break, at 29.53% and 51.49%, respectively. Among the fabricated membranes, CAP 5 mL demonstrated the most balanced overall dialysis performance. Compared with the pristine CS membrane, CAP increased urea and creatinine transport from 28.06% to 61.16% and from 14.34% to 49.68%, while effectively retaining vitamin B12 and BSA, and exhibiting the best overall hemocompatibility, characterized by the lowest hemolysis ratio (0.39%), lowest thrombus formation (40.36%), and the longest PTT (176 seconds). In addition, increasing membrane thickness enhanced hydrophilic interactions and mechanical strength but reduced permeation performance owing to the longer diffusion pathway. These findings identify CAP as a promising membrane for hemodialysis applications and demonstrate that optimizing both membrane composition and thickness is an effective strategy for developing high-performance chitosan-based dialysis membranes. However, further studies under clinically relevant conditions are needed to establish its potential for use in hemodialysis.

Acknowledgment

The authors acknowledge the support of Diponegoro University (Universitas Diponegoro) for providing the research facilities and infrastructure that made this study possible. The authors are also grateful to the faculty members and laboratory staff for their continuous assistance, insightful discussions, and technical support throughout the research.

References

[1] G. T. Lee, Y. K. Hong, Manufacturing and Separation Characteristics of Hemodialysis Membranes to Improve Toxin Removal Rate, *Advances in Polymer Technology*, 2022, 1, (2022), 2565010 https://doi.org/10.1155/2022/2565010

[2] S. Saadati, H. Westphalen, U. Eduok, A. Abdelrasoul, A. Shoker, P. Choi, H. Doan, F. Ein-Mozaffari, N. Zhu, Biocompatibility enhancement of hemodialysis membranes using a novel zwitterionic copolymer: Experimental, *in situ* synchrotron imaging, molecular docking, and clinical inflammatory biomarkers investigations, *Materials Science and Engineering: C*, 117, (2020), 111301 https://doi.org/10.1016/j.msec.2020.111301

[3] O. Azhar, Z. Jahan, F. Sher, M. B. K. Niazi, S. J. Kakar, M. Shahid, Cellulose acetate-polyvinyl alcohol blend hemodialysis membranes integrated with dialysis performance and high biocompatibility, *Materials Science and Engineering: C*, 126, (2021), 112127 https://doi.org/10.1016/j.msec.2021.112127

[4] H. Di, B. Sun, M. Sun, D. Cui, Q. Wang, Thermal reactivity and gas–solid product evolution during coal catalytic combustion: An experimental study, *Journal of Industrial and Engineering Chemistry*, 141,

(2025), 468-476
https://doi.org/10.1016/j.jiec.2024.07.008

[5] I. Geremia, D. Stamatialis, Innovations in dialysis membranes for improved kidney replacement therapy, *Nature Reviews Nephrology*, 16, (2020), 550-551 https://doi.org/10.1038/s41581-020-0293-6

[6] X. Yu, L. Shen, Y. Zhu, X. Li, Y. Yang, X. Wang, M. Zhu, B. S. Hsiao, High performance thin-film nanofibrous composite hemodialysis membranes with efficient middle-molecule uremic toxin removal, *Journal of Membrane Science*, 523, (2017), 173-184 https://doi.org/10.1016/j.memsci.2016.09.057

[7] D. Kim, D. Stamatialis, High flux mixed matrix membrane with low albumin leakage for blood plasma detoxification, *Journal of Membrane Science*, 609, (2020), 118187
https://doi.org/10.1016/j.memsci.2020.118187

[8] A. Nasir, A. Waseh, T. Ahmad, A. Hussain, F. H. Akhtar, Scalable synthesis of asymmetric hemodialysis membranes to enhance performance and biocompatibility in flat sheet and hollow fiber configurations, *Journal of Materials Chemistry B*, 13, 43, (2025), 13954-13971
https://doi.org/10.1039/D5TB01621E

[9] F. Amin, W. Rehman, M. U. Farooq, R. Hussain, S. ur Rahman, L. Rasheed, S. Khan, M. H. Abdellatif, Preparation and Characterization of Biodegradable Cellulose Acetate-Fibroin for Dialysis Application, *ChemistrySelect*, 8, 18, (2023), e202300152
https://doi.org/10.1002/slct.202300152

[10] L. Lin, L. Chen, C. Lu, G. Chen, F. F. Hong, Chitosan particles embedded bacterial nanocellulose flat membrane for hemodialysis, *International Journal of Biological Macromolecules*, 266, (2024), 130646 https://doi.org/10.1016/j.ijbiomac.2024.130646

[11] X. Zhao, D. Chen, N. Zhang, M. Shi, W. Hu, G. Yu, R. Zhao, Biodegradable chitosan zirconium composite adsorptive membranes for potential arsenic (III/V) capture electrodialysis, *International Journal of Biological Macromolecules*, 256, (2024), 128356 https://doi.org/10.1016/j.ijbiomac.2023.128356

[12] M. Ehsani, D. Kalugin, H. Doan, A. Lohi, A. Abdelrasoul, Bio-Sourced and Biodegradable Membranes, *Applied Sciences*, 12, 24, (2022), 12837 https://doi.org/10.3390/app122412837

[13] R. N. Annisa, R. A. Lusiana, G. Gunawan, H. Muhtar, Optimization of Chitosan-Carboxymethyl Chitosan Membrane Modification with PVA to Increase Creatinine and Urea Permeation Efficiency, *Jurnal Kimia Sains dan Aplikasi*, 27, 4, (2024), 189-196 https://doi.org/10.14710/jksa.27.4.189-196

[14] S. B. Rekik, S. Gassara, A. Deratani, Green Fabrication of Sustainable Porous Chitosan/Kaolin Composite Membranes Using Polyethylene Glycol as a Porogen: Membrane Morphology and Properties, *Membranes*, 13, 4, (2023), 378
https://doi.org/10.3390/membranes13040378

[15] R. A. Lusiana, N. A. Sasongko, V. D. A. Sangkota, N. B. A. Prasetya, P. Siahaan, A. A. Kiswandono, M. H. D. Othman, Study of Polysulfone-polyethylene glycol/chitosan (PEG-PSf/CS) Membranes for Urea and Creatinine Permeation, *Jurnal Kimia Sains dan Aplikasi*, 23, 8, (2020), 283-289
https://doi.org/10.14710/jksa.23.8.283-289

[16] R. A. Lusiana, G. A. Pambudi, F. N. Sari, D. S. Widodo, K. Khabibi, S. Isdadiyanto, Grafting of Heparin on Blend Membrane of Citric Acid Crosslinked Chitosan/Polyethylene Glycol-Poly Vinyl Alcohol (PVA-PEG), *Indonesian Journal of Chemistry*, 19, 1, (2019), 151-159 https://doi.org/10.22146/ijc.30861

[17] K. A. Gebru, C. Das, Effects of solubility parameter differences among PEG, PVP and CA on the preparation of ultrafiltration membranes: impacts of solvents and additives on morphology, permeability and fouling performances, *Chinese Journal of Chemistry*, 25, 7, (2017), 911-923 https://doi.org/10.1016/j.cjche.2016.11.017

[18] H. Ritonga, M. Nurdin, L. O. A. N. Ramadhan, Wd S. Salsabila, F. S. Rembon, Preparation of Chitosan Hydrogel with Malonic Acid Crosslinker as Soil Conditioner for Soybean Plant (*Glycine max* L. merril), *Macromolecular Symposia*, 391, 1, (2020), 1900159 https://doi.org/10.1002/masy.201900159

[19] S. Sethi, M. Medha, S. Thakur, D. Sharma, G. Singh, N. Sharma, B. S. Kaith, S. Khullar, Malic acid cross-linked chitosan based hydrogel for highly effective removal of chromium (VI) ions from aqueous environment, *Reactive and Functional Polymers*, 177, (2022), 105318
https://doi.org/10.1016/j.reactfunctpolym.2022.105318

[20] W. Zhang, Q. Jiang, J. Shen, P. Gao, D. Yu, Y. Xu, W. Xia, The role of organic acid structures in changes of physicochemical and antioxidant properties of crosslinked chitosan films, *Food Packaging and Shelf Life*, 31, (2022), 100792
https://doi.org/10.1016/j.fpsl.2021.100792

[21] K. Hab Alrman, S. Alhariri, I. Al- Bakri, Ultrafiltration membrane based on chitosan/adipic acid: Synthesis, characterization and performance on separation of methylene blue and reactive yellow-145 from aqueous phase, *Heliyon*, 10, 11, (2024), e31055
https://doi.org/10.1016/j.heliyon.2024.e31055

[22] T. Martins, E. de S. C. Junior, E. H. M. Nunes, Preparation of chemically crosslinked chitosan hydrogels with adipic acid and EDAC carbodiimide: Tailored biomaterials for multifunctional applications, *Agriculture and Food Sciences Research*, 11, 2, (2024), 187-194
https://doi.org/10.20448/aesr.v11i2.6251

[23] F. Gabriele, A. Donnadio, M. Casciola, R. Germani, N. Spreti, Ionic and covalent crosslinking in chitosan-succinic acid membranes: Effect on physicochemical properties, *Carbohydrate Polymers*, 251, (2021), 117106 https://doi.org/10.1016/j.carbpol.2020.117106

[24] S. K. Bowry, C. Chazot, The scientific principles and technological determinants of haemodialysis membranes, *Clinical Kidney Journal*, 14, Supplement_4, (2021), i5-i16
https://doi.org/10.1093/ckj/sfab184

[25] R. Kono, T. Ota, Y. Kanno, N. Miki, Design of Polyether sulfone flat-sheet membranes for multi-layered hemodiafiltration devices, *PLoS One*, 20, 6, (2025), e0324498
https://doi.org/10.1371/journal.pone.0324498

[26] S. Bhattacharjee, DLS and zeta potential - What they are and what they are not?, *Journal of Controlled*

Release, 235, (2016), 337-351 https://doi.org/10.1016/j.jconrel.2016.06.017

[27] K. Khabibi, D. Siswanta, M. Mudasir, Preparation, characterization, and *in vitro* hemocompatibility of glutaraldehyde-crosslinked chitosan/carboxymethylcellulose as hemodialysis membrane, *Indonesian Journal of Chemistry*, 21, 5, (2021), 1120-1131 https://doi.org/10.22146/IJC.61704

[28] International Organization for Standardization, *Biological Evaluation of Medical Devices—Part 4: Selection of Tests for Interactions with Blood*, International Organization for Standardization, Geneva, Switzerland, 2017

[29] L. Cui, S. Gao, X. Song, L. Huang, H. Dong, J. Liu, F. Chen, S. Yu, Preparation and characterization of chitosan membranes, *RSC Advances*, 8, 50, (2018), 28433-28439 https://doi.org/10.1039/C8RA05526B

[30] I. Popescu, M. Constantin, I. M. Pelin, D. M. Suflet, D. L. Ichim, O. M. Daraba, G. Fundueanu, Eco-Friendly Synthesized PVA/Chitosan/Oxalic Acid Nanocomposite Hydrogels Embedding Silver Nanoparticles as Antibacterial Materials, *Gels*, 8, 5, (2022), 268 https://doi.org/10.3390/gels8050268

[31] R. Sole, C. Buranello, A. Di Michele, V. Beghetto, Boosting physical-mechanical properties of adipic acid/chitosan films by DMTMM cross-linking, *International Journal of Biological Macromolecules*, 209, (2022), 2009-2019 https://doi.org/10.1016/j.ijbiomac.2022.04.181

[32] M. Ji, X. Li, M. Omidvarkordshouli, S. B. Sigurdardóttir, J. M. Woodley, A. E. Daugaard, J. Luo, M. Pinelo, Charge exclusion as a strategy to control retention of small proteins in polyelectrolyte-modified ultrafiltration membranes, *Separation and Purification Technology*, 247, (2020), 116936 https://doi.org/10.1016/j.seppur.2020.116936

[33] K. Lewandowska, M. Szulc, Rheological and Film-Forming Properties of Chitosan Composites, *International Journal of Molecular Sciences*, 23, 15, (2022), 8763 https://doi.org/10.3390/ijms23158763

[34] A. Karydis-Messinis, D. Moschovas, M. Markou, K. Tsirka, C. Gioti, E. Bagli, C. Murphy, A. E. Giannakas, A. Paipetis, M. A. Karakassides, A. Avgeropoulos, C. E. Salmas, N. E. Zafeiropoulos, Hydrogel Membranes from Chitosan-Fish Gelatin-Glycerol for Biomedical Applications: Chondroitin Sulfate Incorporation Effect in Membrane Properties, *Gels*, 9, 11, (2023), 844 https://doi.org/10.3390/gels9110844

[35] W. Chen, V. Karde, T. N. H. Cheng, S. S. Ramli, J. Y. Y. Heng, Surface hydrophobicity: effect of alkyl chain length and network homogeneity, *Frontiers of Chemical Science and Engineering*, 15, (2021), 90-98 https://doi.org/10.1007/s11705-020-2003-0

[36] M. Yan, Q. Bai, Y. Xu, S. Ma, C. Bo, J. Ou, Overview of hemodialysis membranes: Methods and strategies to improve hemocompatibility, *Journal of Industrial and Engineering Chemistry*, 139, (2024), 94-110 https://doi.org/10.1016/j.jiec.2024.05.035

[37] R. A. Lusiana, A. Indra, N. B. A. Prasetya, N. A. Sasongko, P. Siahaan, C. Azmiyawati, N. Wijayanti, A. R. Wijaya, M. H. D. Othman, The Effect of Temperature, Sulfonation, and PEG Addition on Physicochemical Characteristics of PVDF Membranes and Its Application on Hemodialysis Membrane, *Indonesian Journal of Chemistry*, 21, 4, (2021), 942-953 https://doi.org/10.22146/ijc.63740

[38] J. A. del Olmo, J. M. Alonso, V. Sáez-Martínez, S. Benito-Cid, I. Moreno-Benítez, M. Bengoa-Larrauri, R. Pérez-González, J. L. Vilas-Vilela, L. Pérez-Álvarez, Self-healing, antibacterial and anti-inflammatory chitosan-PEG hydrogels for ulcerated skin wound healing and drug delivery, *Biomaterials Advances*, 139, (2022), 212992 https://doi.org/10.1016/j.bioadv.2022.212992

[39] T. N. M. Ismail, N. A. Ibrahim, K. D. P. Palam, A. Sendijarevic, I. Sendijarevic, C. M. Schiffman, S. S. Hoong, M. A. M. Noor, S. K. Yeong, Z. Idris, E. A. Malek, N. Zainuddin, V. Sendijarevic, Effect of Chain Length for Dicarboxylic Monomeric Units of Polyester Polyols on the Morphology, Thermal and Mechanical Properties of Thermoplastic Urethanes, *Journal of the American Oil Chemists' Society*, 97, 7, (2020), 737-749 https://doi.org/10.1002/aocs.12359

[40] R. A. Lusiana, V. D. A. Sangkota, S. J. Santosa, Chitosan succinate/PVA-PEG Membrane: Preparation, Characterization and Permeation Ability Test on Creatinine, *Jurnal Kimia Sains dan Aplikasi*, 21, 2, (2018), 80-84 https://doi.org/10.14710/jksa.21.2.80-84

[41] E. Suryawirawan, A. E. M. Janssen, R. M. Boom, A. van der Padt, Bovine Serum Albumin Rejection by an Open Ultrafiltration Membrane: Characterization and Modeling, *Membranes*, 14, 1, (2024), 26 https://doi.org/10.3390/membranes14010026

[42] P. Cheng, N. Ferrell, S. M. Hus, N. K. Moehring, M. J. Coupin, J. Warner, A.-P. Li, W. H. Fissell, P. R. Kidambi, Protein-Enabled Size-Selective Defect-Sealing of Atomically Thin 2D Membranes for Dialysis and Nanoscale Separations, *Nano Letters*, 25, 1, (2025), 193-203 https://doi.org/10.1021/acs.nanolett.4c04706

[43] M. Mushtaq, M. R. Usmani, N. Hameed, A. Anwar, A. A. Hashmi, Serum Vitamin B12 Deficiency in Chronic Hemodialysis Patients, *Cureus*, 16, 4, (2024), e58751 https://doi.org/10.7759/cureus.58751

[44] M. Soohoo, S.-F. Ahmadi, H. Qader, E. Streja, Y. Obi, H. Moradi, C. M. Rhee, T. H. Kim, C. P. Kovesdy, K. Kalantar-Zadeh, Association of serum vitamin B12 and folate with mortality in incident hemodialysis patients, *Nephrology Dialysis Transplantation*, 32, 6, (2017), 1024-1032 https://doi.org/10.1093/ndt/gfw090

[45] N. A. Sasongko, P. Siahaan, R. A. Lusiana, V. Prasasty, Understanding the interaction of polysulfone with urea and creatinine at the molecular level and its application for hemodialysis membrane, *Journal of Physics: Conference Series*, 1524, 1, (2020), 012084 http://doi.org/10.1088/1742-6596/1524/1/012084

[46] H. B. Park, J. Kamcev, L. M. Robeson, M. Elimelech, B. D. Freeman, Maximizing the right stuff: The trade-off between membrane permeability and selectivity, *Science*, 356, 6343, (2017), https://doi.org/10.1126/science.aab0530

[47] T.-T. Nguyen, H. Fareed, A.-D. Le-Thi, K.-S. Nguyen-Thi, K. Jang, C. S. Kim, S. W. Kim, J. Seo, E. Yang, I. S. Kim, Design of robust hollow fiber membranes using an advanced co-extrusion technology for enhanced hemodialysis, *Chemical*

Engineering Journal, 493, (2024), 152678 https://doi.org/10.1016/j.cej.2024.152678

[48] C. J. O. Bacal, C. J. Munro, B. Tardy, J. W. Maina, J. A. Sharp, J. M. Razal, G. W. Greene, H. H. Nandurkar, K. M. Dwyer, L. F. Dumée, Fouling during hemodialysis – Influence of module design and membrane surface chemistry, *Advanced Membranes*, 4, (2024), 100100 https://doi.org/10.1016/j.advmem.2024.100100

[49] A. Giordano, N. Cancilla, M. Ciofalo, D. Donato, G. Marotta, G. Micale, A. Tamburini, Performance degradation in hollow fiber hemodialysis modules due to blood-induced fouling: experiments and simulations, *Separation and Purification Technology*, 395, (2026), 137853 https://doi.org/10.1016/j.seppur.2026.137853

[50] T. Kiguchi, H. Ito, A. C. Yamashita, Effect of Membrane Surface Area on Solute Removal Performance of Dialyzers with Fouling, *Membranes*, 12, 7, (2022), 684 https://doi.org/10.3390/membranes12070684

[51] P. Melchior, A. Erlenkötter, A. M. Zawada, D. Delinski, C. Schall, M. Stauss-Grabo, J. P. Kennedy, Complement activation by dialysis membranes and its association with secondary membrane formation and surface charge, *Artificial Organs*, 45, 7, (2021), 770-778 https://doi.org/10.1111/aor.13887

[52] William R. Clark, Dayong Gao, Mauro Neri, Claudio Ronco, Solute Transport in Hemodialysis: Advances and Limitations of Current Membrane Technology, in: C. Ronco (Ed.) *Expanded Hemodialysis: Innovative Clinical Approach in Dialysis*, Karger, 2017, https://doi.org/10.1159/000479258

[53] H. Westphalen, A. Abdelrasoul, A. Shoker, Protein adsorption phenomena in hemodialysis membranes: Mechanisms, influences of clinical practices, modeling, and challenges, *Colloid and Interface Science Communications*, 40, (2021), 100348 https://doi.org/10.1016/j.colcom.2020.100348

[54] S. Karla, M. Sorci, B. Moussa, R. Banik, P. B. Petersen, J. Plawsky, G. Belfort, Hydrogen bonds and electrostatics drive adhesion of polar proteins to hydrophilized polymer membranes, *Journal of Colloid and Interface Science*, 701, (2026), 138530 https://doi.org/10.1016/j.jcis.2025.138530

[55] Johanna C. Clauser, Judith Maas, Jutta Arens, Thomas Schmitz-Rode, Ulrich Steinseifer, Benjamin Berkels, Hemocompatibility Evaluation of Biomaterials—The Crucial Impact of Analyzed Area, *ACS Biomaterials Science & Engineering*, 7, 2, (2021), 553-561 https://doi.org/10.1021/acsbiomaterials.0c01589

[56] ASTM International, *Standard Practice for Assessment of Hemolytic Properties of Materials*, 2025, ^https://doi.org/10.1520/F0756-17R25

[57] X. Huang, J. Huang, P. Su, W. Li, Fast Blood Oxygenation through Hemocompatible Asymmetric Polymer of Intrinsic Microporosity Membranes, *Research*, 6, (2023), 0151 https://doi.org/10.34133/research.0151

[58] X. Song, J. Man, Y. Qiu, J. Wang, J. Liu, R. Li, Y. Zhang, J. Li, J. Li, Y. Chen, High-density zwitterionic polymer brushes exhibit robust lubrication properties and high antithrombotic efficacy in blood-contacting medical devices, *Acta Biomaterialia*, 178, (2024), 111-123 https://doi.org/10.1016/j.actbio.2024.02.032

[59] Thomas A. Horbett, Fibrinogen adsorption to biomaterials, *Journal of Biomedical Materials Research Part A*, 106, 10, (2018), 2777-2788 https://doi.org/10.1002/jbm.a.36460

[60] R. Takatsuji, M. Koremoto, Y. Fujimoto, Y. Saida, Y. Hatanaka, Flexible inner surface of polysulfone membranes prevents platelet adhesive protein adsorption and improves antithrombogenicity in vitro, *The International Journal of Artificial Organs*, 47, 10, (2024), 774-782 https://doi.org/10.1177/03913988241269465

[61] Y. Koga, H. Fujieda, H. Meguro, Y. Ueno, T. Aoki, K. Miwa, M. Kainoh, Biocompatibility of Polysulfone Hemodialysis Membranes and Its Mechanisms: Involvement of Fibrinogen and Its Integrin Receptors in Activation of Platelets and Neutrophils, *Artificial Organs*, 42, 9, (2018), E246-E258 https://doi.org/10.1111/aor.13268